Note

The nature of Neptune's increasing brightness: evidence for a seasonal response☆

L.A. Sromovsky,[a],* P.M. Fry,[a] S.S. Limaye,[a] and K.H. Baines[b]

[a] *Space Science and Engineering Center, University of Wisconsin, 1225 W. Dayton Street, Madison, WI 53706, USA*
[b] *Jet Propulsion Laboratory, 4800 Oak Grove Drive, Pasadena, CA 91109, USA*

Abstract

Hubble Space Telescope (HST) observations in August 2002 show that Neptune's disk-averaged reflectivity increased significantly since 1996, by $3.2 \pm 0.3\%$ at 467 nm, $5.6 \pm 0.6\%$ at 673 nm, and $40 \pm 4\%$ in the 850–1000 nm band, which mainly results from dramatic brightness increases in restricted latitude bands. When 467-nm HST observations from 1994 to 2002 are added to the 472-nm ground-based results of Lockwood and Thompson (2002, Icarus 56, 37–51), the combined disk-averaged variation from 1972 to 2002 is consistent with a simple seasonal model having a hemispheric response delay relative to solar forcing of ~30 years (~73% of a full season).
© 2003 Elsevier Science (USA). All rights reserved.

Keywords: Neptune; Neptune, Atmosphere; Meteorology; Atmospheres, dynamics

Introduction

Neptune's equatorial plane is inclined 29° to its orbit plane, which subjects it to seasonal solar forcing during its 164.8-year orbit of the Sun. The resulting local variation in incident sunlight is similar in fractional amplitude to that on the Earth, but the absolute variation is 900 times smaller and the rate of change is an additional factor of 165 slower. Remarkably, there is now evidence that Neptune is responding measurably to this weak forcing. A clear trend of increasing brightness since 1980 has emerged from disk-averaged ground-based observations (Lockwood and Thompson, 2002) and from spatially resolved Hubble Space Telescope (HST) observations in 1996 and 1998 (Sromovsky et al., 2001d). Here we describe new HST observations in 2002, which confirm a continuing increase in

Neptune's reflectivity and establish new constraints on its spectral and spatial characteristics. We show that the recent increase is mainly produced by changes in restricted latitude regions and that the long-term variation follows a simple phase-shifted seasonal model.

Observations

The key HST observations in our analysis, having especially dense longitudinal sampling, were obtained near Neptune's opposition in August 1996 (Sromovsky et al., 2001a), August 1998 (Sromovsky et al., 2001d), and August 2002 (Sromovsky et al., 2002). The best coverage was obtained using HST filters F467M (467 nm), F673N (673 nm), and F850LP (850–1000 nm). Over a time interval spanning 1–3 rotations of Neptune, 9–10 images were acquired for each of these filters for each year. Fig. 1 uses three 673-nm images per year to illustrate the global picture of discrete cloud features and zonal bands, and their changes from 1996 to 2002. The scale at the right shows the relationship of gray levels to reflectivity (I/F) values, which are measured as the ratio of Neptune's radiance to that of a unit-albedo diffuse reflector at the same distance from the Sun. At 673 nm,

* Corresponding author.

E-mail address: larry.sromovsky@ssec.wisc.edu (L.A. Sromovsky).
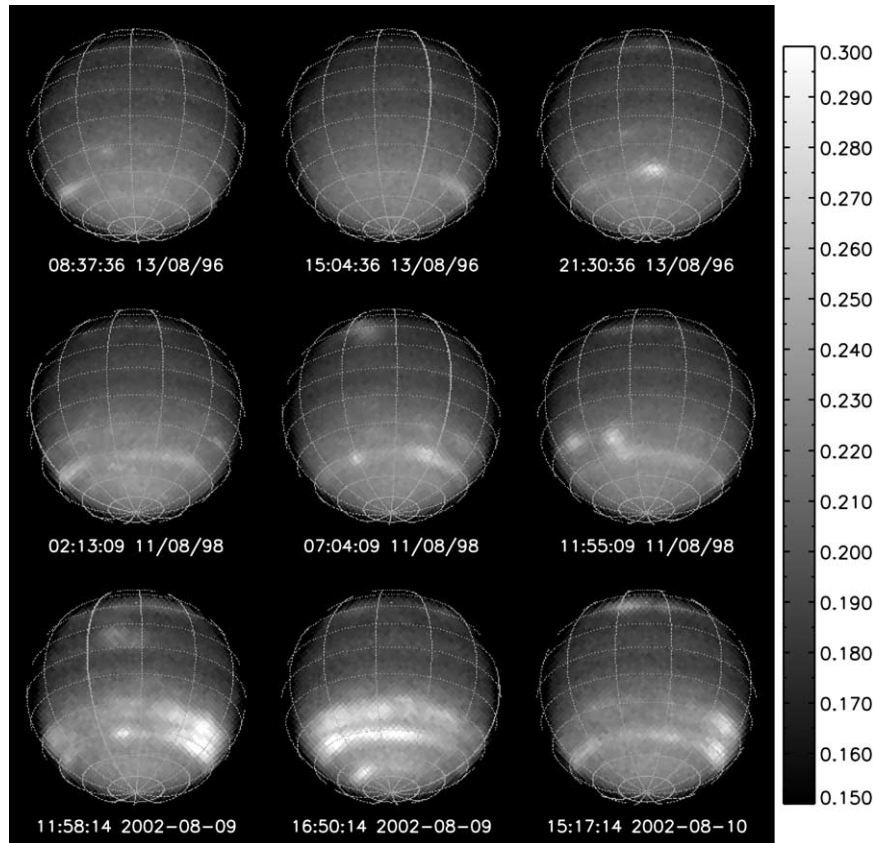
Fig. 1. Images of Neptune at 673 nm, showing discrete cloud features during three HST observing sequences in 1996, 1998, and 2002. During each year three representative images are shown with central meridian longitudes spaced about 120°. The gray-scale labels indicate I/F (reflectivity values), which apply to all images. Grid lines are at intervals of 15° in latitude and 30° in longitude. The images are oriented with Neptune's south pole down.

weak methane band absorption limits our view to about the 5–10 bar level and above (Sromovsky et al., 2001c). Bright cloud features observed in 1996 were found consistently at latitudes of 45°S and somewhat less frequently at 30°S and 30°N. In 1998, the clouds at both southern latitudes were found to be more numerous and a new cloud feature was seen near 67°S, similar to the south polar feature first seen in 1989 Voyager 2 images (Sromovsky et al., 2001a). A much more dramatic change is apparent in the 2002 images, where individual clouds appear to be much brighter at 30°S, 45°S, and 67°S, and the spatial extent of the bright clouds is much greater. This trend is also qualitatively confirmed by Keck observations from July 2000 to June 2001 (Hammel et al., 2001).

Rotational mean results

To characterize the mean behavior of longitude bands we created averages of 9–10 images for each of three filters for each intensive observing year (Fig. 2). Temporal changes seen at 467 nm (top row in Fig. 2) appear subtle because of the high background reflectivity contributed by Rayleigh scattering, which also obscures features deeper than 2–4 bars at this wavelength. At 673 nm (middle row of Fig. 2), reduced Rayleigh scattering permits observations to the 5–10 bar level where methane absorption is the limiting factor. Methane absorption makes Neptune relatively darker overall and increases contrast for the higher altitude bright cloud features. Here we see that cloud bands near 30°S and 45°S have grown significantly in brightness (by 10% or more since 1996) and in latitudinal width (especially at 35°S). For the 850-nm long pass filter (bottom row of Fig. 2), methane absorption is much stronger, providing even greater contrast for bright cloud features, with increases approaching 100% since 1996. The bright clouds observed in 1996 were found to have effective tops ranging from 60 to 230 mb (Sromovsky et al., 2001c), which are plausibly formed from methane ice particles. A widespread optically thin cloud (about 0.15 in optical depth) of methane ice is thought to be present near 1.5 bars (Baines et al., 1995). An H_2S cloud at 3.8 bars may also be present (Baines and Hammel, 1994; Sromovsky et al., 2001c). The increased brightness of the clouds seen in 2002 is likely due to a combination of local changes in the methane clouds, including increases in optical thickness, cloud-top altitude, and fractional coverage.
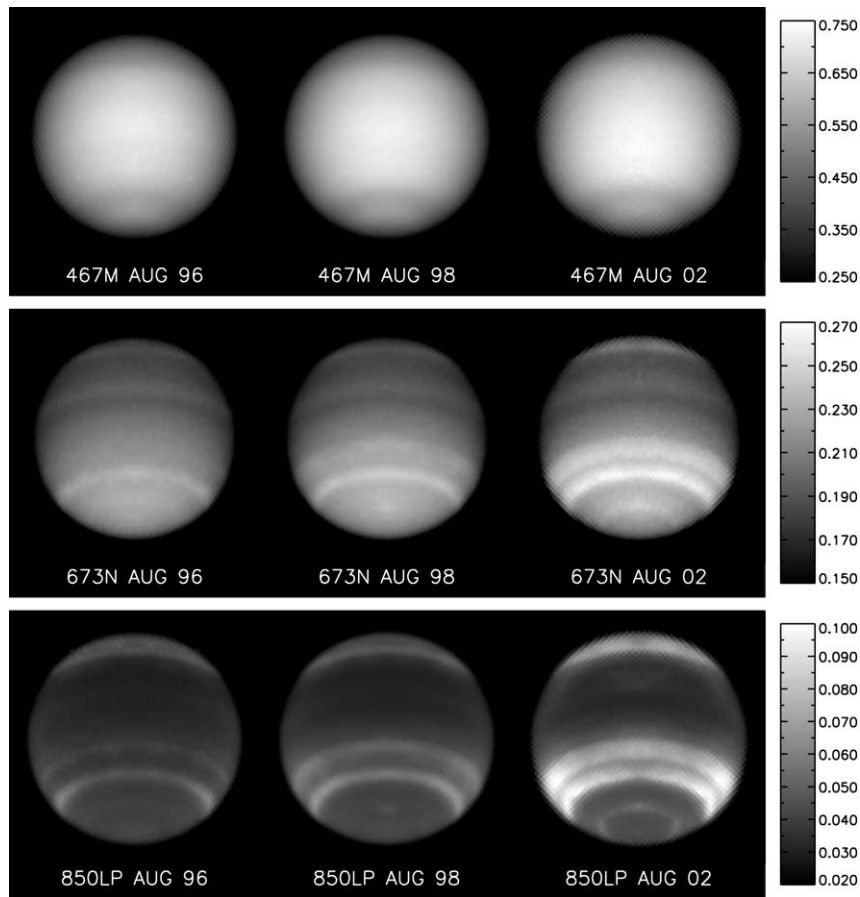
Fig. 2. Averaged HST images of Neptune for 467 nm (top), 673 nm (middle), and 850–1000 nm (bottom), each for 1996 (left column), 1998 (middle), and 2002 (right). The gray-scale relationship to I/F (reflectivity) is indicated at the right for each filter (row).

Disk-averaged results

We computed disk-averaged reflectivity values for the selected HST wavelengths following Sromovsky et al. (2001c) (Figs. 3A–3C). These were corrected to zero phase angle using the factor $1/(1 - \alpha\theta)$, where θ is phase angle and $\alpha = 0.004 \pm 0.004/°$ was estimated from results shown in Fig. 4 of Lockwood and Thompson (2002). We extended the observations for some filters to include HST images from 1994 (Hammel and Lockwood, 1997) and from 2000 and 2001 (Rages et al., 2002), all with somewhat larger errors due to limited rotational lightcurve coverage and uncertainty in phase angle corrections. Not included in the error bars in Fig. 3 are the additional errors inherent to the HST camera system, which is estimated to have a relative accuracy for ratios within 1% over a period of 4 years (Bagget and Gonzaga 1998). This uncertainty is indicated by the pair of dotted curves surrounding the 467-nm trend line. The linear regression results for the rates of increase in reflectivity at HST wavelengths are, in order of wavelength, $0.0030 \pm 0.0003/y$, $0.0020 \pm 0.0002/y$, and $0.0027 \pm 0.0002/y$, which are remarkably similar in absolute value. Expressed as percentages of 1996 values, the slopes are 0.53%/year, 0.95%/year, and 6.6%/year. The respective ac-

cumulated changes from 1996 to 2002 are thus 3.2, 5.6, and 40%.

Also shown in Fig. 3A are *b*-filter ground-based observations of Lockwood and Thompson (2002). The *b* filter (λ = 471 nm, $\Delta\lambda$ = 20 nm) is a close match to the HST WFPC2 F467M filter in both width and central wavelength. The close tracking of HST and ground-based observations (within 0.1–0.2%) is remarkable, considering that different instruments and different calibration systems are used. It is also significant, given the historical record of Neptune's variability, that these two different sets of samples, both covering generally short periods, which sparsely sample Neptune's variation at different mean times, should display such a smooth time dependence.

Longer-term changes in Neptune's disk-averaged reflectivity are shown in Fig. 3D, where 1972–2000 ground-based observations (Lockwood and Thompson, 2002) at 472 nm are plotted with HST observations at 467 nm, with both normalized to their respective August 1996 values. From 1972 to 1980 Neptune's reflectivity appeared to correlate well with solar UV variations during the 11-year solar cycle (Lockwood and Thompson, 2002, 1986; Baines and Smith, 1990). But from 1980 to 2000, Neptune brightened continuously, by 11% at 472 nm, with most of the increase coming
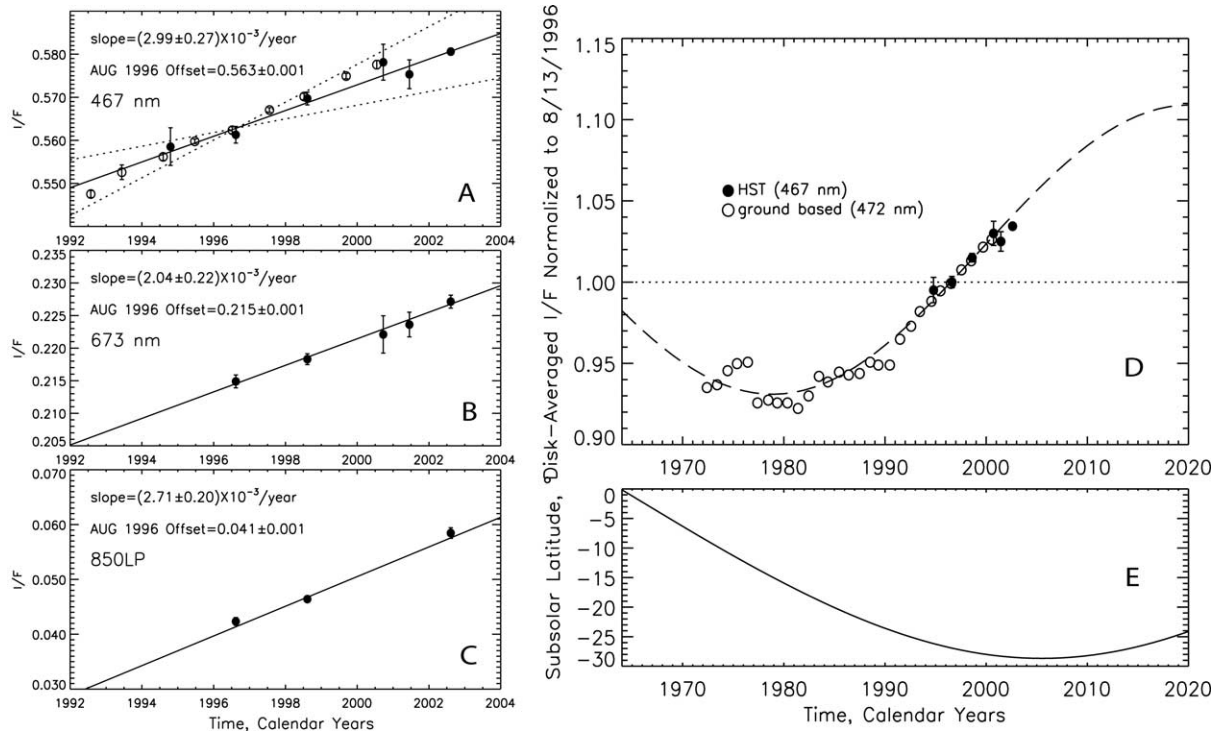
Fig. 3. Neptune's disk-averaged reflectivity versus time for three HST filters: F467M (A), F673N (B), and F850LP (C). The open circles in A indicate 472-nm (*b*-filter) ground-based results of Lockwood and Thompson (2002). Long-term disk-averaged reflectivity of Neptune (D), as inferred by 1972–2000 ground-based observations at 472 nm (open circles), and from 467-nm HST observations (filled circles) from 1994 through 2002. The best-fit seasonal model (dashed curve) has its peak delayed 15.1 years relative to the upcoming hemispheric solar forcing peak in 2005, when the subsolar latitude (E) will be at its southern extreme.

after 1990. The time period where HST and ground-based observations overlap seems to be a period of reduced short-term variability. The general shape of the long-term variation is consistent with a seasonal response.

A seasonal model of disk-averaged I/F

A simple seasonal response model can be constructed by initially assuming that Neptune's summer hemisphere exhibits the greatest dynamical activity and cloud brightness when it gets the maximum exposure to sunlight, i.e., at the summer solstice, and the least activity and brightness at the winter solstice. This would produce a brightness peak in each hemisphere at its summer solstice, when it would also be most visible from the Earth. The brightness minima would then occur at the equinoxes, when both hemispheres would be at mid-brightness and equally visible from the Earth. However, Neptune's effective temperature of 59 K makes it a very weak radiator and thus prevents rapid equilibrium with the varying solar input. Instead there would be a delayed thermal (and presumed cloud brightness) response to the solar forcing, with a phase delay of ϕ = arctan ($\omega \tau_R$), where $\omega = 2\pi/T$ is the angular frequency of Neptune's orbit, T is Neptune's orbital period, and τ_R is the radiative relaxation time (Conrath et al., 1990). At potentially relevant pressure levels of 30, 100, and 500 mb,

expected thermal response phase shifts are 63°, 84°, and 75°, the largest equaling that observed for Titan (Sromovsky et al., 1991). These are all significant fractions of the maximum of 90° (a full season).

The combination of view angle variations and delayed cloud response to solar forcing leads to the following approximate model for the disk-averaged reflectivity,

$$I(t) = I_o[(1/2 + a \sin(\omega t))(1 + b \sin(\omega t - \phi))$$
$$+ (1/2 - a \sin(\omega t))(1 - b \sin(\omega t - \phi))], \quad (1)$$

where t is time after the southern hemisphere spring equinox (1964), a is the amplitude of variation of the fractional solid angle occupied by a given hemisphere's contributing region, and b is the fractional amplitude of variation in reflectivity of a given hemisphere. The first term inside the square brackets describes the contribution of the southern hemisphere and the second gives that of the northern hemisphere. This can be reduced to the simpler relative form

$$I(t)/<I> = 1 - d \cos(2\omega t - \phi), \quad (2)$$

where $d = 1/[(ab)^{-1} + \cos(\phi)]$ and $<I> = I_o (1 + ab \cos(\phi))$. The peaks in southern hemisphere solar forcing in this model occur at $t_{SF} = T/4 \pm nT$, and the peaks in southern hemisphere brightness response at $t_{SR} = T \phi/(2\pi) + T/4 \pm nT$. The corresponding northern hemisphere peaks are offset by time T and the peaks in disk-integrated re-

sponse occur at $t_{DR} = T\phi/(4\pi) + T/4 \pm nT/2$. The delay in either hemisphere's response to its solar forcing is $t_{SR} - t_{SF} = T\phi/(2\pi)$, and the delay in the disk-integrated peak from the last hemispheric solar forcing peak is given by $t_{DR} - t_{SF} = T\phi/(4\pi)$. As shown in Fig. 3D, this model provides good fits to the combined b-filter and 467-nm observations for $d = 0.089 \pm 0.004$ and $\phi = 66° \pm 2°$, which is between phase delay values expected at 30 and 500 mb (Conrath et al., 1990). The corresponding time delays for this fit are $t_{SR} - t_{SF} = 30.2$ years and $t_{DR} - t_{SF} = 15.1$ years, leading to a disk-averaged peak around 2020.

Discussion: implications of near-IR correlations

Lockwood and Thompson (2002) found a strong correlation between their b-filter observations and the IR J-band (1.25 μm) observations made near the time of the 1976 outburst (Joyce et al., 1977; Cruikshank, 1978). The IR fractional variation was larger than the b-filter variation by factors of 20 to 50 depending on whether the variations are matched over 60 days or 3 years, respectively. That would lead us to expect the IR brightness of Neptune to be much greater now and also in 1996 than it was in 1976. But 1996 IRTF (InfraRed Telescope Facility) observations of Neptune (Sromovsky et al., 2001b) show that the IR brightness then was actually smaller than in 1976. It appears that visible and IR observations are seeing different aspects of the long-term variation, even though there are substantial short-term correlations. A possible explanation is suggested by an unusual spectral difference in 1996 rotational lightcurves (Sromovsky et al., 2001b). Lightcurves of very similar shapes were found at 673 nm, 893 nm, and 1.25 μm (J), with fractional amplitudes of 1.7, 22, and 55%, respectively. These lightcurves were all dominated by discrete bright clouds. However, the 467-nm lightcurve was very different: not only was its amplitude much smaller ($\sim$0.5%), but its shape was also very nearly the inverse of the other lightcurves. While the rotational variation for most filters was controlled by bright features, the variation at 467 nm was found to be dominated by a circumpolar wave feature that was only dark at blue wavelengths. Although Figs. 3A–3C show that increases in bright clouds were clearly the dominant source of long-term variations at all wavelengths after 1996, we expect that dark features at 467 nm were more visible or more prominent during earlier years. At the seasonal minimum we speculate that dark features compensated at 467 nm for much of the high-altitude cloud contributions that dominated both long-term and short-term variations at longer wavelengths.

Discussion: conflicting observations

Although our simple seasonal model fits most disk-integrated observations at 467 and 472 nm well, it is not con-

sistent with the local brightness increase beyond 30°N (Fig. 2), especially between 1998 and 2002; that hemisphere ought to be declining in overall brightness according to the seasonal model. However, this is a minor feature and might be just a short-term local variation. A potentially more serious conflict is suggested by the Lockwood and Thompson (2002) compilation of early ground-based observations in a broadband (B) filter (Hardie and Giclas, 1955; Jerzykiewicz and Serkowski, 1966), which indicate that Neptune's brightness during 1950–1966 increased about 1–2% between 1950 and 1960, while the seasonal model would imply a decrease of about 10%. However, the nominal B filter (Lockwood and Thompson 2002) spans a wavelength range from 390 to 500 nm (half-maximum points), which is about five to six times the width of the b filter and is much more heavily weighted toward shorter wavelengths, with a peak response near 412 nm when the spectral response of the typical photomultiplier tube is also accounted for (Johnson and Morgan, 1951). It is conceivable that the B measurements recorded a combination of decreasing I/F at longer wavelengths (due to decreasing cloud reflectivity) and a more rapidly increasing I/F at shorter wavelengths (due to decreasing stratospheric haze absorption). Clearly some variation in Neptune's spectrum is required to explain the near-IR results discussed in the previous paragraph. However, it does not seem likely that the effect at short wavelengths could be large enough by itself to explain the entire discrepancy. Another potential source for unusual brightness changes is the heightened solar activity near the end of 1957 when the largest-ever monthly mean sunspot number was observed (sunspot data from ftp://ftp.ngdc.noaa.gov). Sunspot number was anticorrelated with Neptune's brightness during the 1972–1980 period when it seemed to be associated with 2–3% variations in brightness (Lockwood and Thompson, 1986). But during 1950–1961, the B-filter observations of a steadily increasing brightness contain no evidence of a 1957 minimum that would have been obvious had the same correlation been present then as during 1972–1980. Thus, the B observations during 1950–1960 seem inconsistent with both seasonal and solar responses. An alternate possibility is that these earlier broadband measurements are in error, either due to instrumental anomalies or analysis errors. In fact, Jerzykiewicz and Serkowski (1966) themselves raise this issue by pointing out that "The steady decrease of the instrumental coefficient A_8 in the years 1950–1960 . . . throws some doubt on the reality of the changes in Neptune's brightness." A clear resolution of this discrepancy remains to be found.

It should be noted that the discrepancies between the seasonal model and the observations are mainly with observations that are minor in effect or made in different spectral bands and that very good agreement is obtained with the best-calibrated and most spectrally homogeneous disk-averaged observations. Thus, seasonal forcing remains a plausible explanation for Neptune's main brightness variation, although a firm understanding of the complete variation and

all its contributing factors and spectral variation remains to be established. Achieving that understanding will probably require a much longer record of observations and more detailed investigations of physical mechanisms. If the seasonal model is correct, Neptune should continue to brighten at 467 nm for almost another two decades.

References

Bagget, S., Gonzaga, S., 1998. WFPC2 long-term stability. Instrument Science Report WFPC 98-03, available from the Space Telescope Science Institute (www.stsci.edu).

Baines, K.H., Smith, W.H., 1990. The atmospheric structure and dynamical properties of Neptune derived from ground-based and IUE spectrophotometry. Icarus 85, 65–108.

Baines, K.H., Hammel, H.B., 1994. Clouds, hazes, and the stratospheric methane abundance in Neptune. Icarus 109, 20–39.

Baines, K.H., Hammel, H.B., Rages, K.A., Romani, P.N., Samuelson, R.E., 1995. Clouds and hazes in the atmosphere of Neptune, in: Cruikshank, D.P. (Ed.), Neptune and Triton. Univ. of Arizona Press, Tucson, pp. 489–546.

Conrath, B.J., Gierasch, P.J., Leroy, S.S., 1990. Temperature and circulation in the stratosphere of the outer planets. Icarus 83, 255–281.

Hardie, R.H., Giclas, H.L., 1955. A search for solar variations. Astrophys. J. 122, 460–465.

Hammel, H.B., Lockwood, G.W., 1997. Atmospheric structure of Neptune in 1994, 1995, and 1996. Icarus 129, 466–481.

Hammel, H.B., Rages, K., Lockwood, G.W., 2001. Observations of Neptune in 2000 and 2001. Bull. Am. Astron. Soc. 33, 1403–1404.

Jerzykiewicz, M., Serkowski, K., 1966. The Sun as a variable star. III. Lowell Obs. Bull. 6, 295–323.

Johnson, H.L., Morgan, W.W., 1951. On the color-magnitude diagram of the Pleiades. Astrophys. J. 114, 522–543.

Lockwood, G.W., Thompson, D.T., 1986. Long-term brightness variations of Neptune and the solar cycle modulation of its albedo. Science 234, 1543–1545.

Lockwood, G.W., Thompson, D.T., 2002. Photometric variability of Neptune, 1972–2000. Icarus 156, 37–51.

Rages, K., Hammel, H.B., Lockwood, G.W., 2002. A prominent apparition of Neptune's south polar feature. Icarus 159, 262–265.

Smith, B.A., et al., 1989. Voyager 2 at Neptune: imaging science results. Science 246, 1422–1449.

Sromovsky, L.A., Suomi, V.E., Pollack, J.B., Krauss, R.J., Limaye, S.S., Owen, T., Revercomb, H.E., Sagan, C., 1981. Implications of Titan's north-south brightness asymmetry. Nature 292, 698–702.

Sromovsky, L.A., Fry, P.M., Baines, K.H., Limaye, S.S., Orton, G.S., Dowling, T.E., 2001a. Coordinated 1996 HST and IRTF imaging of Neptune and Triton. I. Observations, navigation, and deconvolution techniques. Icarus 149, 416–434.

Sromovsky, L.A., Fry, P.M., Baines, K.H., Dowling, T.E., 2001b. Coordinated 1996 HST and IRTF imaging of Neptune and Triton. II. Implications of disk-integrated photometry. Icarus 149, 435–458.

Sromovsky, L.A., Fry, P.M., Dowling, T.E., Baines, K.H., Limaye, S.S., 2001c. Coordinated 1996 HST and IRTF imaging of Neptune and Triton. III. Neptune's atmospheric circulation and cloud structure. Icarus 149, 459–488.

Sromovsky, L.A., Fry, P.M., Dowling, T.E., Baines, K.H., Limaye, S.S., 2001d. Neptune's atmospheric circulation and cloud morphology: changes revealed by 1998 HST images. Icarus 150, 244–260.

Sromovsky, L.A., Fry, P.M., Baines, K.H., Limaye, S.S., 2002. HST observations of Neptune in 2002. Bull. Am. Astron. Soc. 34, 858.